Amoeba Active Contours

Martin Welk

Institute for Biomedical Image Analysis
University for Health Sciences, Medical Informatics and Technology
Eduard-Wallnöfer-Zentrum 1, 6060 Hall/Tyrol, Austria
martin.welk@umit.at
http://ibia.umit.at

Abstract. We introduce an algorithm for active contour segmentation in which the level set function encoding the contour is processed by median filtering using morphological amoebas. These are adaptive structure elements introduced by Lerallut et al. which can be combined with different morphological operations. Recently it has been proven that iterated amoeba median filtering of an image approximates the well-known self-snakes partial differential equation. Following this approach we prove a partial approximation property of amoeba active contours with respect to geodesic active contours. Experiments prove the viability of the algorithm and confirm the theoretical results.

1 Introduction

The concept of morphological amoebas for structure-adaptive morphological filtering has been introduced by Lerallut et al. [19,20]. In this approach, structure elements adapt flexibly to image structures by taking into account spatial distance of pixels as well as image contrast. By penalising large deviations in image values, amoebas can grow around corners or along anisotropic image features. Once amoeba structure elements are constructed, a great variety of morphological filters can be applied.

One candidate for the filtering step is median filtering which assigns to each pixel the median of all grey-values of the given image within the structure element as its new grey-value. A classic result by Guichard and Morel [13] establishes a relation to partial differential equation (PDE) based image filtering: In its continuous-scale limit median filtering approximates mean curvature motion [2], i.e. the PDE $u_t = |\nabla u| \operatorname{div}(\nabla u/|\nabla u|)$.

Median filtering with amoeba structure elements has been investigated in [19,20]. In [29] it was proven that iterated amoeba median filtering approximates the self-snakes image filter PDE [23,30], i.e. that a space-continuous formulation of amoeba median filtering asymptotically equals a time step of the self-snakes evolution. As in [13] the time step size goes to zero with the square of the radius of the structure element (amoeba).

Self-snakes stand in close relationship to *geodesic active contours* [9,15], a well-established PDE method for image segmentation. In view of the approximation

A.M. Bruckstein et al. (Eds.): SSVM 2011, LNCS 6667, pp. 374–385, 2012.

property between amoeba median filtering and self-snakes it is natural to ask whether a similar amoeba-based process can be designed that performs an active contour segmentation. In this paper, we will demonstrate that this is indeed possible and that the resulting algorithm has similar properties as geodesic active contours. For a special case we will prove an approximation property in the same sense as in [13,29]. While the main contribution of the present paper is of theoretical nature, the new discrete approach to active contours might also turn out useful in applications because nonstandard discretisations of this kind may reduce e.g. numerical dissipation effects that are difficult to circumvent with finite-difference schemes.

Related work. The discrete filters that are in the focus of the present paper take their motivation from two sources: first, the classic median filter as introduced by Tukey [26] which has developed into a standard tool in image processing later on, see e.g. [16]; second, the idea of image-adaptive structure elements [6,7,24,28] which also includes Lerallut et al.'s morphological amoebas [19,20]. The space-continuous description of amoebas resorts to the representation of an image by an image manifold which has been used in the context of the Beltrami framework [14,31] and also underlies the bilateral filter [3,25].

Geodesic active contours were formulated by Caselles et al. [9] and Kichenassamy et al. [15], based on earlier work on active contours [8,21].

The paradigmatic PDE approximation result by Guichard and Morel [13] for the median filter has been followed by results for further discrete filters [3,11,27], for amoeba median filtering see [29].

Structure of the paper. In Section 2 we describe morphological amoebas and develop the amoeba active contour algorithm. By a space-continuous analysis in Section 3 approximation of the geodesic active contour PDE is proven in the radially symmetric case. Experiments demonstrate the viability of the approach, and its similarity to geodesic active contours, see Section 4. Conclusions are presented in Section 5.

2 Amoeba Active Contour Filtering

Let us recall first the principle of amoeba filters as introduced in [19,20].

The first step of any amoeba filter consists in the construction of image-adaptive structure elements, called amoebas, for all pixels in the image. The structure element for pixel p is made up by those pixels which are close to p in some *amoeba metric*. Instead of considering only the spatial distance in the image domain, as for non-adaptive morphological structure elements, the amoeba metric measures the distance of pixels along the *image manifold,* i.e. a surface interpolating the $\mathbb{R}^3$ points $(x, y, \sigma f(x, y))$. Here, (x, y) are point coordinates in the image domain, $f(x, y)$ is the grey-value at (x, y), and the scaling parameter $\sigma > 0$ weights grey-value differences (tonal distances) against spatial distances.

In the second step, some morphological operation is applied to the image with the previously computed structure elements, such as dilation, erosion, opening or

closing. As a particularly interesting example, median filtering has been studied in [19,20,29]. Like the non-adaptive median filter, this filter can be iterated, giving rise to *iterated amoeba median filtering.*

Space-discrete and space-continuous amoeba metrics. Concerning the amoeba metric, let us discuss first the space-continuous setting. Natural choices for the Riemannian metric on the image manifold $\{(x, y, \sigma f(x, y))\}$ are those induced by metrics in the embedding space $\mathbb{R}^3$. The simplest case, the Euclidean metric, leads to the amoeba metric $\mathrm{d}s^2 = \mathrm{d}_2 s^2 = \mathrm{d}x^2 + \mathrm{d}y^2 + \sigma^2 \mathrm{d}f^2$. An alternative is an L^1 metric $\mathrm{d}s = |\mathrm{d}x| + |\mathrm{d}y| + \sigma|\mathrm{d}f|$ which, however, lacks the desirable rotational invariance in space and will not be considered further here. As a compromise, one can choose a combined L^2-L^1 metric that is Euclidean in the two spatial dimensions but L^1 in combining the spatial and tonal distances, $\mathrm{d}s = \mathrm{d}_1 s = \sqrt{\mathrm{d}x^2 + \mathrm{d}y^2} + \sigma|\mathrm{d}f|$. A straightforward generalisation is

$$\mathrm{d}s = \mathrm{d}_\varphi s = \varphi\left(\sqrt{\mathrm{d}x^2 + \mathrm{d}y^2}, \sigma\,\mathrm{d}f\right) \tag{1}$$

where φ is a twice differentiable nonnegative function, homogeneous of degree 1, strictly increasing in both variables, and fulfils the triangle inequality, see [29].

The distance $d(p, q)$ between two points $p = (x_p, y_p, \sigma f_p)$, $q = (x_q, y_q, \sigma f_q)$ on the image manifold is the minimum of the expression

$$L_\varphi(C) := \int_C \mathrm{d}_\varphi s\ , \tag{2}$$

taken over all curves C on the image manifold that connect p and q. Note, however, that for $q \to p$ and smooth u, this distance is asymptotically equal to the corresponding distance of p and q in $\mathbb{R}^3$, i.e.

$$d(p, q) \approx \varphi\left(\sqrt{(x_p - x_q)^2 + (y_p - y_q)^2}, \sigma|f_p - f_q|\right)\ . \tag{3}$$

In a digitised image, a space-discrete formulation of the distance measurement is used. Following [19,20,29] $d(p, q)$ is the minimum of

$$L_\varphi(c) := \sum_{k=0}^{m-1} \varphi\left(\sqrt{(x_k - x_{k+1})^2 + (y_k - y_{k+1})^2}, \sigma|f_k - f_{k+1}|\right) \tag{4}$$

over all discrete curves $(p_0 = p, p_1, \ldots, p_m = q)$, where $p_k = (x_k, y_k, \sigma f_k)$. A discrete curve is a sequence of points in which each pair of subsequent points are neighbours in the image domains. In [19,20], this model is used with $\mathrm{d}_\varphi \equiv \mathrm{d}_1$ and 4-neighbourhoods, while [29] uses general d_φ and 8-neighbourhoods. We will follow the latter model, notwithstanding that, as [29] mentions, accuracy could be further improved by digital distance transforms [4,5,17,18].

Active contours. In an active contour algorithm [8,21], a contour curve evolves from some initial shape towards a shape that separates the given image into two

segments (typically, a foreground object and the background). The initial shape is provided either by user interaction or some automatic method.

The evolution equation for *geodesic active contours* [9,15] is given by

$$c_t = (g(|\nabla f|)\kappa - \langle \nabla g(|\nabla f|), \boldsymbol{n} \rangle)\, \boldsymbol{n} \tag{5}$$

where $\boldsymbol{n}$ is the inward normal vector, and κ the curvature of the contour curve c. The nonnegative "edge-stopping function" g depends monotonically decreasing on the local gradient of the input image f. The name *geodesic* active contours indicates that the contour found by this evolution is a local minimum of the arc length, thus, a geodesic, in some image-dependent metric.

The contour c that evolves according to (5) can be represented in different ways, which leads to different implementations of the active contour method. The concept of a contour as parametric curve leads to a representation by sample points. This is on one hand comparably efficient since it represents a curve as a truly one-dimensional object; on the other hand, the evolution of sample points to inter-pixel positions necessitates interpolation. Moreover, due to length changes of the evolving curve over- and undersampling occurs, requiring re-sampling steps in the algorithms. Further difficulties are encountered when segments with multiple connected components cause the need for topology changes in the contour.

Alternatively, level-set methods [22] represent the contour c as zero-level set of a function u over the two-dimensional image domain. For example, a signed distance function of the contour can serve this purpose. The evolution equation (5) is then rewritten into an evolution of $u = u(x, y, t)$ as

$$u_t = |\nabla u| \operatorname{div}\left(g(|\nabla f|)\frac{\nabla u}{|\nabla u|}\right) = g(|\nabla f|)u_{\xi\xi} + \langle \nabla g, \nabla u \rangle \tag{6}$$

where ξ denotes a unit vector in level line direction of u, $\xi \perp \nabla u$. Topology changes are implicitly handled in this case, and resampling becomes a non-issue. However, the numerical evaluation in a 2D spatial domain raises the computational cost. This can be mitigated by narrow-band approaches [1] that restrict the computation to the immediate neighbourhood of the actual contour.

In all cases, the contour evolution takes place under the influence of the image being segmented; the image itself is not changed in this process.

Here lies the difference between active contours (snakes) and *self-snakes.* A self-snakes evolution is obtained from an active contour evolution in level-set formulation by identifying the level-set function for the contour with the image, thereby evolving the image itself.

Active contour filtering using morphological amoebas. To design an amoeba-based algorithm for active contours, the identification of input image and evolving image must be removed, leading to the following procedure:

1. Compute amoeba structure elements based on the input image f.
2. Initialise the evolving image u with a level-set function for the initial contour.

3. Evolve the image u by median filtering with the amoebas from Step 1 as structure elements.

In contrast to the iterated amoeba median filtering as described in [29], amoebas depend on the immutable input image and are therefore computed just once for the entire evolution. This saves computational expense and opens the way for further computational optimisations.

Introduction of dilation/erosion terms. Particularly if the initial contour is far from the actual segment boundary, and if the segment boundary is of complex topology, the geodesic active contour evolution (5) or (6) can stop in an undesired local minimum away from the desired contour. For such cases it is recommended in the literature [10,15] to modify (5) by an additional force term $\pm\nu\boldsymbol{n}$. This "balloon force" resembles morphological dilation or erosion and pushes the evolution into a chosen direction, thereby preventing it from stopping prematurely in regions with little contrast.

A similar behaviour can be achieved in the amoeba-based active contour model. To this end, one can bias the median filter: Instead of always selecting the element with index $m/2$ within the ordered sequence $g_0, \ldots, g_m$ of the grey-values in the amoeba, one chooses the element with index αm for some $\alpha \neq 1/2$ (the α-quantile), or the element with index $m/2 + b$ with some fixed offset b. We will use the latter modification in one of our experiments.

3 Space-Continuous Analysis

We turn now to analysing the amoeba active contour filter in a space-continuous setting, and aim at establishing a relationship to a PDE formulation. Analogous to the proceeding in [29], we approximate the input image f and the level-set function u locally by Taylor expansions up to second order, and compute then approximately the amoeba shape, and the median of u within that shape.

For the purposes of the present contribution, we restrict ourselves to the Euclidean amoeba metric $d_\varphi \equiv d_2$. We will not carry out an analysis in full generality but consider the special case in which the input image and initial contour are radially symmetric, which in particular implies that the level lines of the level-set function u and of the input image f always coincide. This special case is motivated by the idea that relevant parts of the segment boundary found by an active contour evolution should be almost aligned with level lines of the input image. Also, analysis of the biased method is beyond the scope of the present paper.

We consider expansions of σf and u within a ϱ-neighbourhood of $(x_0, y_0) = (0, 0)$. Here, $(0, 0)$ is not the centre of radial symmetry; we assume that ∇u and ∇f do not vanish at this point. Without loss of generality, we assume $u(0, 0) = 0$, $f(0, 0) = 0$, and assume that the gradients of u and f are in x direction. The Taylor expansions of u and f then read

$$\sigma f(x, y) = \alpha x + \gamma x^2 + \delta y^2 + \mathcal{O}(\varrho^3) \tag{7}$$

$$u(x, y) = \mu x + \nu x^2 + \lambda y^2 + \mathcal{O}(\varrho^3)\ . \tag{8}$$

Due to the required radial symmetry the mixed monomial xy does not occur. By the locally invertible coordinate transform $z = \mu x + \nu x^2 + \lambda y^2$ we obtain

$$\sigma f = \frac{\alpha}{\mu} z + \frac{\beta}{\mu^2} z^2 + \mathcal{O}(\varrho^3) \tag{9}$$

$$u = z + \mathcal{O}(\varrho^3) \,. \tag{10}$$

Note that the curvatures of level lines of σf and u are equal, such that the coordinate transform straightens not only the level lines of u but also those of σf, making the y^2 contribution vanish.

The contour of the amoeba $\mathcal{A}$ with centre $p = (0, 0)$ and amoeba radius ϱ is made up by all those points $q = (x, y)$ for which $d_2(p, q) = \varrho^2$, i.e. $x^2 + y^2 + (\sigma f(x, y))^2 - \varrho^2 = \mathcal{O}(\varrho^4)$ or

$$y^2 \left(1 - \frac{2\lambda}{\mu^2} z\right) + \left(\frac{1+\alpha^2}{\mu^2} z^2 + 2\left(\frac{\alpha\beta}{\mu^3} - \frac{\nu}{\mu^4}\right) z^3\right) - \varrho^2 = \mathcal{O}(\varrho^4) \,. \tag{11}$$

A given level line $u = z$ of u intersects the contour of $\mathcal{A}$ in two points. Their y coordinates are solutions of (11), understood as quadratic equation for y, i.e. $y = \pm Y(z) + \mathcal{O}(\varrho^3)$ with

$$Y(z) = \sqrt{\varrho^2 - \frac{1+\alpha^2}{\mu^2} z^2} \left(1 + \frac{\lambda}{\mu^2} z - \frac{\alpha\beta/\mu^3 - \nu/\mu^4}{\varrho^2 - (1+\alpha^2) z^2/\mu^2} z^3\right) \,. \tag{12}$$

Thus, the length of the level line segment within $\mathcal{A}$ is up to $\mathcal{O}(\varrho^3)$ equal to $2Y(z)$. It is nonnegative for $z \in [Z_-, Z_+]$ where

$$Z_\pm = \pm \frac{\varrho\mu}{\sqrt{1+\alpha^2}} + \mathcal{O}(\varrho^2) \,, \tag{13}$$

and goes to zero with $\mathcal{O}(\sqrt{|z - Z_\pm|})$ when approaching the boundaries.

The part of the amoeba $\mathcal{A}$ in which u takes values $z \in [a, b] \subseteq [Z_-, Z_+]$ has an area approximately given by the integral $2\int_a^b Y(z)\tau(z)\,\mathrm{d}z$ where $\tau(z) := \partial x/\partial z = 1/\mu - 2\nu z/\mu^2 + \mathcal{O}(\varrho^2)$ represents the inverse density of level lines. The median M of u within $\mathcal{A}$ therefore satisfies the condition

$$\int_{Z_-}^{M} Y(z)\tau(z)\,\mathrm{d}z = \int_{M}^{Z_+} Y(z)\tau(z)\,\mathrm{d}z + \mathcal{O}(\varrho^4) \,, \tag{14}$$

which yields, with a loss of accuracy due to the approximation of the integration boundaries via (13),

$$\int_0^{\varrho\mu/\sqrt{1+\alpha^2}} \big(Y(z)\tau(z) - Y(-z)\tau(-z)\big)\,\mathrm{d}z = 2\int_0^M Y(z)\tau(z)\,\mathrm{d}z + \mathcal{O}(\varrho^{7/2}) \,. \tag{15}$$

Since $M = \mathcal{O}(\varrho^2)$ and $Y(0) = \varrho$, we have $\int_0^M Y(z)\tau(z)\,\mathrm{d}z = \varrho M/\mu + \mathcal{O}(\varrho^4)$, and by the substitution $z = \varrho\mu\zeta/\sqrt{1+\alpha^2}$ we obtain

$$\begin{aligned} M &= \frac{(\lambda - 2\nu)\varrho^2}{1+\alpha^2} \int_0^1 \zeta\sqrt{1-\zeta^2}\,\mathrm{d}\zeta - \frac{(\alpha\beta\mu + \nu)\varrho^2}{(1+\alpha^2)^2} \int_0^1 \frac{\zeta^3\,\mathrm{d}\zeta}{\sqrt{1-\zeta^2}} + \mathcal{O}(\varrho^{5/2}) \\ &= \frac{\varrho^2}{6}\left(\frac{2\lambda - 4\nu}{1+\alpha^2} - \frac{4\alpha\beta\mu - 4\nu}{(1+\alpha^2)^2}\right) + \mathcal{O}(\varrho^{5/2})\,. \end{aligned} \tag{16}$$

Based on the expansions (9), (10) and the variable substitution for z we can express the coefficients in terms of derivatives of u and f. We have $\mu = u_x$, $\nu = \frac{1}{2}u_{xx}$, $\lambda = \frac{1}{2}u_{yy}$, $\alpha = \sigma f_x$, $\beta = \gamma - \alpha\nu/\mu = \frac{\sigma}{2}\,(f_{xx} - f_x u_{xx}/u_x)$. Giving up our special choice of coordinates, we replace x and y by unit vectors $\eta \parallel \nabla f$ and $\xi \perp \nabla f$ in gradient and level line direction, respectively. Thus the last equation expresses that, in the radially symmetric case, one step of the amoeba active contour filter asymptotically approximates for $\varrho \to 0$ one time step of size $\varrho^2/6$ of an explicit scheme for the PDE

$$u_t = \frac{u_{\xi\xi}}{1+\sigma^2|\nabla f|^2} - \frac{2\sigma^2 f_\eta f_{\eta\eta} u_\eta}{(1+\sigma^2|\nabla f|^2)^2} = g(|\nabla f|)u_{\xi\xi} + \langle \nabla g(|\nabla f|), \nabla u\rangle\,, \tag{17}$$

i.e. (6) with the Perona-Malik-type edge stopping function (compare [9,15])

$$g(s) := (1+\sigma^2 s^2)^{-1}\,. \tag{18}$$

It is still an open question whether this approximation property holds in exactly the same form for situations other than the radially symmetric case discussed here. Nevertheless, even this partial equivalence result links amoeba active contours to the framework of PDE active contour methods and makes it an interesting candidate for a non-standard discrete realisation of active contours.

4 Experiments

Our first experiment (Figure 1) demonstrates the viability of the amoeba active contour approach and its similarity to geodesic active contours. Starting from an initial contour that generously surrounds almost the entire image area of the test image, Figure 1(a), our amoeba active contour algorithm adapts to the outline of the depicted human head section within 600 iterations with amoeba radius 10, see Figure 1(b, c). By our approximation result (16) the corresponding evolution time for an active contour PDE is $T = 10000$.

Indeed, computation of geodesic active contours (6) up to $T = 10000$ by an explicit finite difference scheme gives a similar result, see Figure 1(d). Slight differences, in particular a stronger rounding of contours, can be attributed to the blurring effect of the central difference approximation of derivatives.

The theoretical link between amoeba active contours and geodesic active contours established in Section 3 is rooted in a space-continuous setting. In fact,

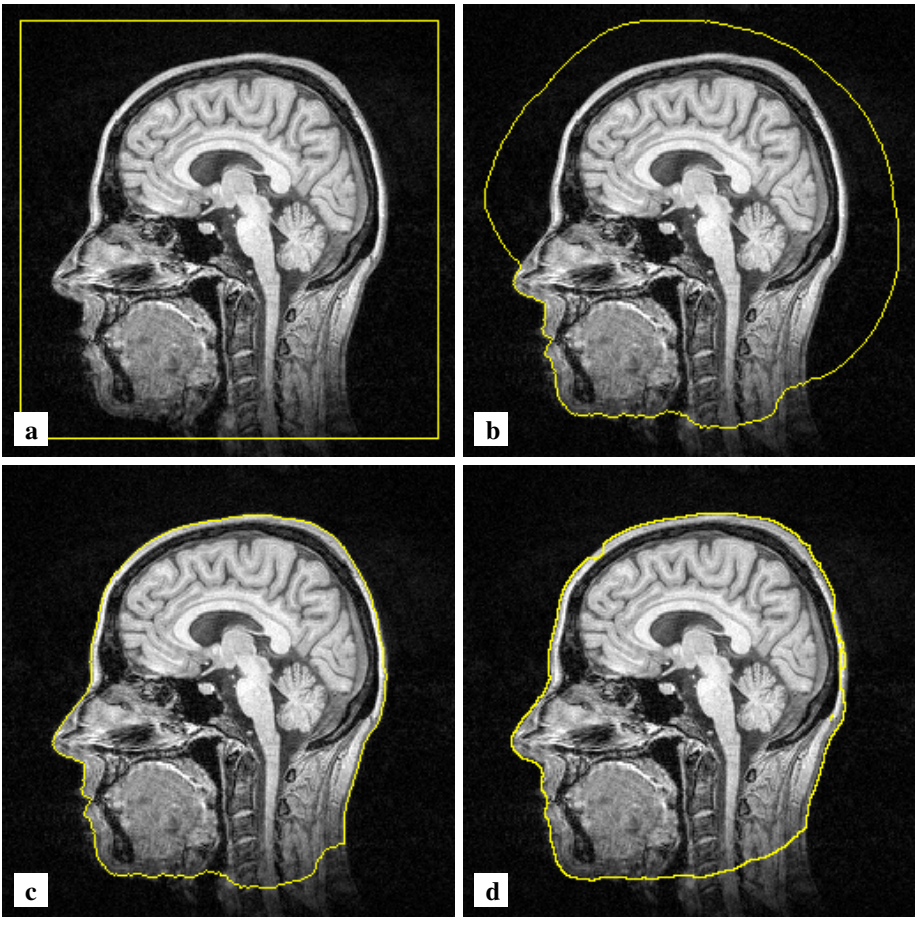

Fig. 1. (a) MR image of a human head with initial contour. **(b)** Amoeba active contours (unbiased), amoeba radius $\varrho = 10$, $\sigma = 0.1$, 200 iterations. **(c)** Amoeba active contours, same parameters but 600 iterations. **(d)** Geodesic active contours (6) with edge-stopping function (18), $\sigma = 0.1$, computed by an explicit time-stepping scheme with time step size $\tau = 0.25$, 40000 iterations.

the application of both filters to digital images reveals some differences in detail which can be attributed to their fundamentally different discrete realisation. The already mentioned numerical dissipation of finite difference discretisations stands in contrast to the very fine adaptivity of amoeba shapes to image structures, which is also reflected in the resulting active contours.

Furthermore, while the disposition to "lock in", i.e. become stationary at image structures with strong gradients, is a feature of both active contour approaches, such a behaviour is more pronounced in the case of amoeba active contours. The reason is that the underlying median filter already in its non-adaptive formulation possesses non-constant steady states, so called root signals [12].

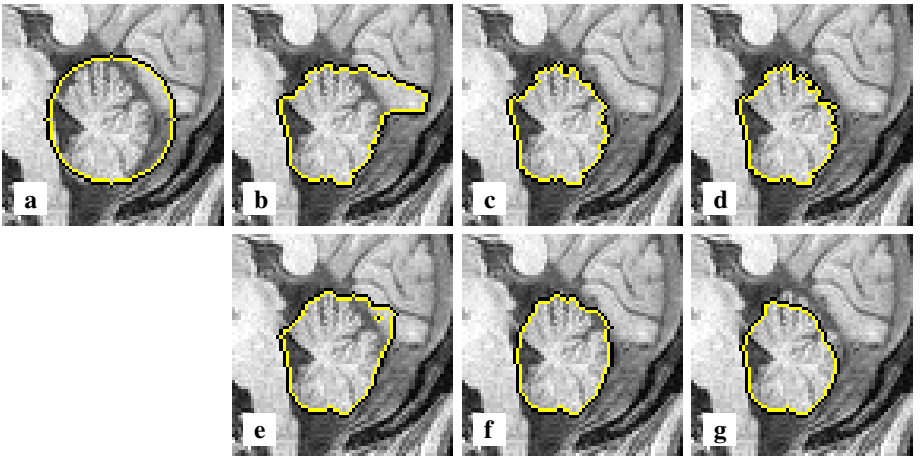

Fig. 2. (a) MR image with initial contour (detail). **(b)** Amoeba active contours (unbiased), amoeba radius $\varrho = 10$, $\sigma = 0.1$, 20 iterations. **(c)** Same but $\varrho = 12$, $\sigma = 0.1$, 10 iterations. **(d)** Same but $\varrho = 12$, $\sigma = 0.1$, 60 iterations. **(e)** Geodesic active contours (6), $\sigma = 0.1$, $\tau = 0.25$, 960 iterations. **(f)** Same but 3000 iterations. **(g)** Same but 57600 iterations.

It is therefore natural also for an amoeba median filter to develop root signals, the more if the amoeba shapes themselves are kept fixed as in our case. This property contributes on one hand to stabilising the segmentation result. On the other hand it means that some minimal amoeba size is needed for reasonable segmentation. Experiments suggest that ϱ should not be smaller than 10.

As speed optimisation has not been in the focus of our work so far, a proper comparison of the two active contour algorithms in terms of runtimes cannot be made at this point. To this end, additional optimisation effort for both algorithms would be required. To state a rough trend we mention that in our present, non-optimised implementations both algorithms are roughly comparable in speed, the amoeba-based algorithm being about 15 % faster than the PDE scheme in the case of Figure 1(c) vs. (d) (but sometimes also a bit slower in other examples).

In our second experiment (Figure 2) we use the same test image as before but aim at segmenting the cerebellum. As our initial contour, Figure 2(a), is not very precise, the amoeba active contour with amoeba radius $\varrho = 10$, the amoeba active contour locks in at some sharp contours outside the desired region (b). With a slightly enlarged amoeba radius $\varrho = 12$ a fairly good segmentation is reached (c). Further evolution of the amoeba contours becomes stationary at a contour that cuts off some small details (d). Running geodesic active contours up to evolution time $T = 240$ (which matches the amoeba evolution of the third frame above) still does not segment the cerebellum well (e); this is achieved only after considerably longer evolution time (f). Continuing geodesic active contour evolution, again a stationary contour is reached, see Figure 2(g).

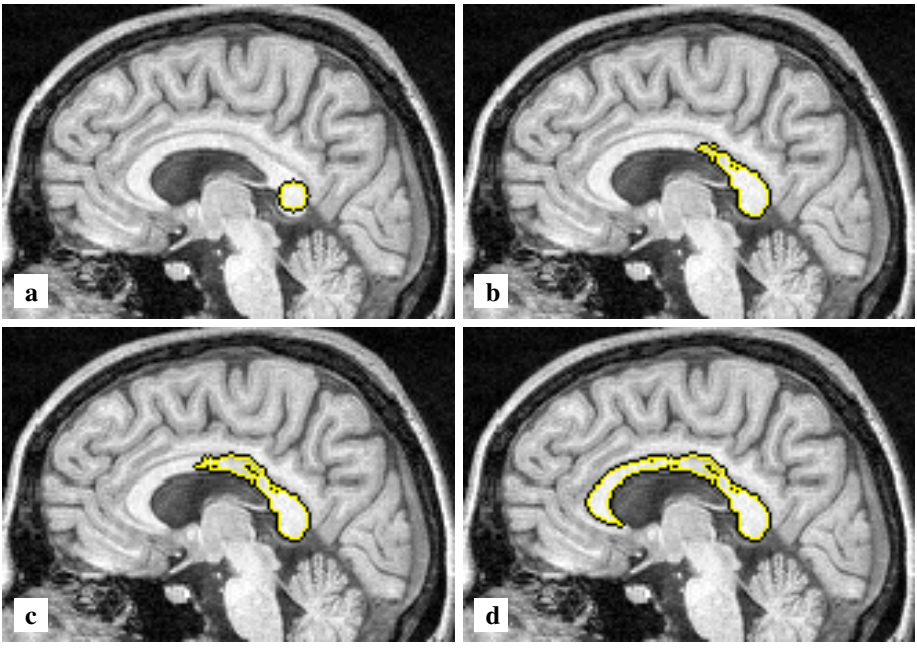

Fig. 3. **(a)** MR image with initial contour (detail). **(b)** Amoeba active contours with dilation bias, amoeba radius $\varrho = 20$, $\sigma = 2.0$, bias $b = 10$, 5 iterations. The bias $b = 10$ means that within each amoeba the 10-th greyvalue above the median index was chosen. **(c)** Same but 15 iterations. **(d)** Same but 30 iterations.

In our third experiment (Figure 3) we demonstrate the modification of amoeba active contours by a dilation bias $b = 10$ in order to force an expansive evolution of the contour. Thus, within each increasing sequence of grey-values of an amoeba the value 10 positions after the median was selected (the maximum if the amoeba contained less than 20 pixels). Together with amoeba radius $\varrho = 20$ and a comparatively large contrast parameter $\sigma = 2.0$ this allowed to segment the corpus callosum from a small initial contour within the structure.

5 Conclusion

In this paper we have developed a new variant of an active contour algorithm for image segmentation based on iterated amoeba median filtering of a level-set function. We proved that in a radially symmetric setting the continuous-scale limit of our amoeba active contour method coincides with the well-known geodesic active contour equation. Experiments verify that both algorithms behave structurally similar. Due to their entirely different discrete filter strategies, they differ in the representation of contour details.

Ongoing work is directed at extending our theoretical analysis. This will include the study of non-radially symmetric situations as well as different amoeba

metrics and the relation between the biased approach and additional force terms. A further goal are algorithmic optimisations.

The revenue of this effort will be, firstly, a deeper theoretical insight into the relations between discrete and continuous image filters will be gained. Secondly, based on the so established approximation properties genuinely discrete filters can be used as unconventional discretisations of PDE filters and improve the practical implementation of the latter.

Acknowledgements. The author thanks Michael Breuß for helpful discussions on the topic. Implementation is partially based on earlier work by Oliver Vogel.

References

1. Adalsteinsson, D., Sethian, J.A.: A fast level set method for propagating interfaces. Journal of Computational Physics 118(2), 269–277 (1995)
2. Alvarez, L., Lions, P.-L., Morel, J.-M.: Image selective smoothing and edge detection by nonlinear diffusion. II. SIAM Journal on Numerical Analysis 29, 845–866 (1992)
3. Barash, D.: Bilateral filtering and anisotropic diffusion: Towards a unified viewpoint. In: Kerckhove, M. (ed.) Scale-Space 2001. LNCS, vol. 2106, pp. 273–280. Springer, Heidelberg (2001)
4. Borgefors, G.: Distance transformations in digital images. Computer Vision, Graphics and Image Processing 34, 344–371 (1986)
5. Borgefors, G.: On digital distance transforms in three dimensions. Computer Vision and Image Understanding 64(3), 368–376 (1996)
6. Braga-Neto, U.M.: Alternating sequential filters by adaptive neighborhood structuring functions. In: Maragos, P., Schafer, R.W., Butt, M.A. (eds.) Mathematical Morphology and its Applications to Image and Signal Processing. Computational Imaging and Vision, vol. 5, pp. 139–146. Kluwer, Dordrecht (1996)
7. Breuß, M., Burgeth, B., Weickert, J.: Anisotropic continuous-scale morphology. In: Martí, J., Benedí, J.M., Mendonça, A.M., Serrat, J. (eds.) IbPRIA 2007. LNCS, vol. 4478, pp. 515–522. Springer, Heidelberg (2007)
8. Caselles, V., Catté, F., Coll, T., Dibos, F.: A geometric model for active contours in image processing. Numerische Mathematik 66, 1–31 (1993)
9. Caselles, V., Kimmel, R., Sapiro, G.: Geodesic active contours. In: Proc. Fifth International Conference on Computer Vision, pp. 694–699. IEEE Computer Society Press, Cambridge (1995)
10. Cohen, L.D.: On active contour models and balloons. Computer Vision, Graphics, and Image Processing: Image Understanding 53(2), 211–218 (1991)
11. Didas, S., Weickert, J.: Combining curvature motion and edge-preserving denoising. In: Sgallari, F., Murli, A., Paragios, N. (eds.) SSVM 2007. LNCS, vol. 4485, pp. 568–579. Springer, Heidelberg (2007)
12. Eckhardt, U.: Root images of median filters. Journal of Mathematical Imaging and Vision 19, 63–70 (2003)
13. Guichard, F., Morel, J.-M.: Partial differential equations and image iterative filtering. In: Duff, I.S., Watson, G.A. (eds.) The State of the Art in Numerical Analysis. IMA Conference Series (New Series), vol. 63, pp. 525–562. Clarendon Press, Oxford (1997)

14. Kimmel, R., Sochen, N., Malladi, R.: Images as embedding maps and minimal surfaces: movies, color, and volumetric medical images. In: Proc. 1997 IEEE Computer Society Conference on Computer Vision and Pattern Recognition, pp. 350–355. IEEE Computer Society Press, San Juan (1997)
15. Kichenassamy, S., Kumar, A., Olver, P., Tannenbaum, A., Yezzi, A.: Gradient flows and geometric active contour models. In: Proc. of Fifth International Conference on Computer Vision, pp. 810–815. IEEE Computer Society Press, Cambridge (1995)
16. Klette, R., Zamperoni, P.: Handbook of Image Processing Operators. Wiley, New York (1996)
17. Ikonen, L.: Priority pixel queue algorithm for geodesic distance transforms. Image and Vision Computing 25(10), 1520–1529 (2007)
18. Ikonen, L., Toivanen, P.: Shortest routes on varying height surfaces using gray-level distance transforms. Image and Vision Computing 23(2), 133–141 (2005)
19. Lerallut, R., Decencière, E., Meyer, F.: Image processing using morphological amoebas. In: Ronse, C., Najman, L., Decencière, E. (eds.) Mathematical Morphology: 40 Years On. Computational Imaging and Vision, vol. 30. Springer, Dordrecht (2005)
20. Lerallut, R., Decencière, E., Meyer, F.: Image filtering using morphological amoebas. Image and Vision Computing 25(4), 395–404 (2007)
21. Malladi, R., Sethian, J.A., Vemuri, B.C.: A topology independent shape modeling scheme. In: Vemuri, B. (ed.) Geometric Methods in Computer Vision. Proceedings of SPIE, vol. 2031, pp. 246–258. SPIE Press, Bellingham (1993)
22. Osher, S., Sethian, J.A.: Fronts propagating with curvature-dependent speed: Algorithms based on Hamilton–Jacobi formulations. Journal of Computational Physics 79, 12–49 (1988)
23. Sapiro, G.: Vector (self) snakes: a geometric framework for color, texture and multiscale image segmentation. In: Proc.1996 IEEE International Conference on Image Processing, Lausanne, Switzerland, vol. 1, pp. 817–820 (September 1996)
24. Shih, F.Y., Cheng, S.: Adaptive mathematical morphology for edge linking. Information Sciences 167(1–4), 9–21 (2004)
25. Tomasi, C., Manduchi, R.: Bilateral filtering for gray and color images. In: Proc. Sixth International Conference on Computer Vision, pp. 839–846. Narosa Publishing House, Bombay (1998)
26. Tukey, J.W.: Exploratory Data Analysis. Addison–Wesley, Menlo Park (1971)
27. van den Boomgaard, R.: Decomposition of the Kuwahara–Nagao operator in terms of linear smoothing and morphological sharpening. In: Talbot, H., Beare, R. (eds.) Mathematical Morphology: Proc. Sixth International Symposium, pp. 283–292. CSIRO Publishing, Sydney (2002)
28. Verly, J.G., Delanoy, R.L.: Adaptive mathematical morphology for range imagery. IEEE Transactions on Image Processing 2(2), 272–275 (1993)
29. Welk, M., Breuß, M., Vogel, O.: Morphological amoebas are self-snakes. Journal of Mathematical Imaging and Vision (in press, 2011)
30. Whitaker, R.T., Xue, X.: Variable-conductance, level-set curvature for image denoising. In: Proc. 2001 IEEE International Conference on Image Processing, Thessaloniki, Greece, pp. 142–145 (October 2001)
31. Yezzi Jr., A.: Modified curvature motion for image smoothing and enhancement. IEEE Transactions on Image Processing 7(3), 345–352 (1998)